https://doi.org/10.5194/egusphere-2025-4308
Preprint. Discussion started: 16 September 2025

Impact of model resolution and turbulence scheme on the representation of mountain waves and turbulence

Roshny Siri Jagan[1] and Juerg Schmidli[1]

[1]Goethe University, Frankfurt

Correspondence: Roshny Siri Jagan (roshnyjagan@gmail.com)

Abstract. Simulating mountain waves and associated turbulence in the upper troposphere and lower stratosphere (UTLS) remains a challenge in numerical weather prediction (NWP). We investigate how the representation of mountain-wave dynamics and turbulence in the ICOsahedral Nonhydrostatic (ICON) model depends on model resolution and turbulence parameterization. ICON simulations were performed in NWP mode (ICON-NWP) with varying horizontal (2 km, 1 km, 500 m) and vertical (400 m, 200 m, 100 m) resolutions, using the operational turbulent kinetic energy scheme and the newly developed two-energy turbulence scheme. The simulations were evaluated against high-frequency in situ observations from the Deep Propagating Gravity Wave Experiment (DEEPWAVE) over New Zealand on 12 July 2014, as well as nested large-eddy simulations (ICON-LES) at 130 m resolution. The results show reasonable agreement with observations: ICON-LES more closely captures wavelength and phase, while ICON-NWP better reproduces wave amplitude. Near-convergence of local wave and turbulence structures requires horizontal grid spacings of 1 km or finer and vertical spacings in the UTLS of 200 m or finer. A key finding is that both turbulence schemes yield similar wave structures, despite large differences in simulated turbulent kinetic energy. This discrepancy is primarily attributed to the empirical parameterization of the horizontal shear term, which may not be realistic at very high resolutions. In terms of bulk measures, the area-averaged gravity-wave momentum flux approaches convergence already at 1 km. These results provide guidance on the resolution and turbulence representation needed for reliable simulations of small-scale mountain waves and turbulence in the UTLS.

1 Introduction

The upper troposphere and lower stratosphere (UTLS), spanning roughly 6 to 25 km altitude (Riese et al., 2012), plays a central role in climate dynamics by regulating the distribution of greenhouse gases. As a transition zone between the relatively well-mixed troposphere and the stably stratified lower stratosphere, the UTLS facilitates tracer transport through a range of dynamical processes operating across multiple spatial and temporal scales (Scherllin-Pirscher et al., 2021; Riese et al., 2012). These processes include the large-scale Brewer–Dobson circulation (months to years), Rossby wave breaking and baroclinic cyclones (several days), deep convection on shorter timescales (Schäfler et al., 2023), and small-scale turbulence. Turbulence in the UTLS is particularly important for stratosphere–troposphere exchange of chemical constituents. Unlike the planetary boundary layer, where turbulence is sustained, turbulence aloft is intermittent and localized, producing short-lived but intense

https://doi.org/10.5194/egusphere-2025-4308
Preprint. Discussion started: 16 September 2025

mixing events, especially near the tropopause (Mirza et al., 2024). Acting on horizontal scales of a few hundred meters to several kilometers, UTLS turbulence can significantly influence large-scale circulation patterns (Rogel et al., 2023).

Upper-air turbulence in the UTLS can be broadly categorized by its origin into three types: clear-air turbulence, often associated with jet streams; mountain-wave turbulence (MWT), generated by flow over topography; and convectively induced turbulence, linked to thunderstorms (Kim et al., 2023; Ren and Lynch, 2024). Among these, MWT is of particular importance because it poses substantial challenges for aviation safety, flight planning, and route optimization (Mahalov, 2016). Many long-haul flight routes cross major mountain ranges, where MWT occurs frequently and often with high intensity. Understanding mountain-wave dynamics and their associated turbulence is therefore not only relevant for weather and climate research, but also for operational forecasting and aviation risk management.

Mountain waves are a specific type of gravity wave that arises when stably stratified air is forced to flow over topography, producing oscillations with gravity as the restoring force. As these waves propagate upward, their amplitude increases with decreasing air density. When the intrinsic phase speed of the wave approaches the background wind speed, the wave amplitude reaches a maximum and momentum is transferred to the mean flow. Beyond this point, the wave can become unstable and generate turbulence. This occurs either through catastrophic wave breaking, in which the wave is completely destroyed, or through wave saturation, where energy is dissipated into turbulence that limits further amplitude growth. In the latter case, the wave only partially breaks but still produces localized turbulent mixing. These processes illustrate the close coupling of gravity waves and turbulence, which is central to understanding energy and momentum transfer in the UTLS (Arbor, 1999; Schneider et al., 2017; Dörnbrack et al., 1995; Sharman et al., 2012; Fritts and Alexander, 2003).

Mountain waves play a major role in atmospheric energetics by transporting energy and momentum away from their source regions. They are typically generated in the troposphere and can propagate both vertically into the stratosphere and horizontally over long distances. The structure and propagation of a mountain wave depend strongly on the size and shape of the underlying topography as well as on the vertical profiles of wind, temperature, and moisture in the flow (Durran, 2015). Orographic gravity waves often dominate the global gravity-wave spectrum, with momentum fluxes several times larger than those of non-orographic waves and concentrated over regions of complex terrain (Holt et al., 2017).

Mountain waves have been investigated extensively through ground-based instruments, in situ aircraft measurements, satellite observations, and dedicated field campaigns (Heale et al., 2022; Grubišić and Lewis, 2004; Grubišić et al., 2008; Bougeault et al., 1993; Kuettner and O'Neill, 1981; Bougeault et al., 2001; Wratt et al., 1996; Fritts et al., 2016; Schäfler et al., 2018; Jackson et al., 2018; Rapp et al., 2021). These studies have identified several "hotspots" of gravity-wave activity, such as regions downstream of major mountain ranges (Heale et al., 2022). Despite this rich observational record, forecasting mountain waves and associated turbulence in numerical weather prediction (NWP) and climate models remains highly challenging. The difficulty arises from the multiscale interactions between waves and turbulence, and from the fact that a large part of the gravity-wave spectrum lies below the typical grid resolution of global models and thus must be parameterized (Plougonven et al., 2020; Achatz et al., 2024; Voelker, 2024). Recent advances in computational power have enabled mesoscale nested simulations with horizontal resolutions of about 1 km or finer, offering new opportunities to explicitly resolve small-scale processes

https://doi.org/10.5194/egusphere-2025-4308
Preprint. Discussion started: 16 September 2025

while still accounting for the large-scale environment provided by coarser parent domains (Muños-Esparza et al., 2020; Rogel et al., 2023).

Large-eddy simulation (LES) and direct numerical simulation (DNS) provide powerful tools for investigating turbulence associated with mountain waves at very high resolution. These approaches can resolve small-scale structures that remain inaccessible to operational NWP models. For example, Bramberger et al. (2020) used a two-dimensional model with 200 m horizontal and 100 m vertical grid spacing to simulate a mountain-wave breaking event over Iceland. Their results demonstrated that the observed turbulence could be attributed directly to breaking mountain waves. Such high-resolution studies highlight the potential of LES and DNS to improve physical understanding of mountain-wave turbulence, while also providing valuable benchmarks for evaluating parameterizations in coarser-resolution models.

Several recent modeling studies have addressed the resolution required to capture mountain-wave dynamics and associated processes with fidelity. Lund et al. (2020) and Fritts et al. (2021) investigated the nonlinear evolution of mountain waves over the southern Andes using simulations at 500 m resolution, revealing the complex dynamics that emerge with increasing wave forcing. Extending this work, Fritts et al. (2022) examined how model resolution affects the representation of mountain waves propagating into the thermosphere. Their results showed that coarser resolutions quickly degrade the ability to simulate key wave dynamics, leading to systematic biases in global models that influence both weather and climate predictions. Through simulations of wintertime flow over the southern Andes at horizontal resolutions ranging from 0.5 to 8 km, they demonstrated that resolutions of about 2 km or finer are necessary to adequately capture mountain-wave responses, particularly in the mesosphere.

Most turbulence parameterizations used in numerical models were originally developed for the atmospheric boundary layer (ABL), but they are not necessarily suited to conditions in the UTLS. The ABL is characterized by a solid lower boundary and strongly influenced by diurnal cycles of radiative heating and cooling, leading to turbulence generation mechanisms that differ fundamentally from those aloft. In contrast, turbulence in the UTLS occurs in a strongly stratified environment, is often patchy and anisotropic, and appears as sudden, localized bursts of velocity and temperature fluctuations that deviate from classical Kolmogorov scaling (Rodriguez Imazio et al., 2023; Kleeorin et al., 2019; Mahalov, 2016; Paoli et al., 2014). The challenges of applying ABL-based schemes at kilometer-scale resolutions in the UTLS have been demonstrated by Muños-Esparza et al. (2020), who showed that turbulence parameterization significantly influences gravity-wave activity and vertical mixing in high-resolution weather simulations. Using a case of widespread turbulence over the U.S. Great Plains, they found that a 1 km model tends to overestimate vertical velocities, wave fluxes, and kinetic energy compared to a 250 m LES. These findings underline the need for turbulence parameterizations adapted specifically to UTLS conditions in order to capture wave–turbulence interactions more realistically.

In this study, we evaluate the performance of two turbulence schemes implemented in the ICOsahedral Nonhydrostatic (ICON) limited-area model for simulating mountain waves and associated turbulence in the UTLS. Specifically, we compare the operational turbulent kinetic energy scheme (ICON-TKE) with the newly developed two-energy turbulence scheme (ICON-2TE). Sensitivity experiments are conducted with varying horizontal and vertical resolutions to determine the model configuration required to capture key wave and turbulence characteristics. The simulations are qualitatively evaluated against

https://doi.org/10.5194/egusphere-2025-4308
Preprint. Discussion started: 16 September 2025

high-frequency in situ observations from the Deep Propagating Gravity Wave Experiment (DEEPWAVE), a field campaign conducted over New Zealand in 2014, and against nested large-eddy simulations (ICON-LES) at 130 m resolution. The remainder of the paper is organized as follows: Sect. 2 describes the ICON model setup, including the two turbulence schemes, the case study, and the analysis methodology. Sect. 3 presents the evaluation of a reference simulation and the results of the sensitivity experiments, including a discussion of their implications for simulating mountain waves and turbulence in the UTLS. Finally, Sect. 4 summarizes the main findings and provides recommendations for future work.

2 Experimental setup

2.1 Case study and observational data

The case analyzed in this study is a mountain-wave event over New Zealand on 12 July 2014 during the DEEPWAVE campaign. This case is useful because it combines a clearly observed mountain wave with relatively rare high-frequency in situ measurements near the tropopause. Earlier analyses inferred possible signatures of turbulence impacts on tracer distributions in the UTLS region (Lachnitt et al., 2023). Although direct observational evidence of wave breaking was not available, the event provides targeted in situ observations that make it suitable for evaluating how turbulence parameterizations and model resolution affect the simulation of mountain waves in the UTLS.

The synoptic situation during the event was characterized by a trough to the west of New Zealand and a weak low-pressure system to the south of the islands. This configuration produced moderate northwesterly flow across the South Island, i.e., about $10\,\mathrm{m\,s^{-1}}$ to $15\,\mathrm{m\,s^{-1}}$ at $5\,\mathrm{km}$, oriented perpendicular to the Southern Alps. At tropopause level (around $10\,\mathrm{km}$ altitude, $250\,\mathrm{hPa}$), winds were also from the northwest, reaching moderate speeds of about $20\,\mathrm{m\,s^{-1}}$ along the DEEPWAVE flight path. Overall, weak directional shear created favorable conditions for the generation of vertically propagating mountain waves over the South Island.

The DEEPWAVE research flight FF09 was carried out with the DLR Falcon aircraft on 12 July 2014 between 17:15 and 20:15 UTC. The aircraft followed a clockwise rectangular flight track across the South Island to capture the structure of the mountain-wave event (see Fig. 1). To sample vertical variability, the flight pattern consisted of two stacked legs separated by approximately $75\,\mathrm{min}$, with the lower level at $360\,\mathrm{hPa}$ ($7.9\,\mathrm{km}$) and the upper level at $230\,\mathrm{hPa}$ ($10.9\,\mathrm{km}$). In the southern segment of the track, the lower leg was flown between 17:30 and 17:50 UTC and the corresponding upper leg between 18:47 and 19:06 UTC. In the northern segment, the lower leg took place from 18:12 to 18:32 UTC and the upper leg from 19:27 to 19:47 UTC. These stacked cross sections provide in situ measurements of mountain waves and turbulence signatures near the tropopause and serve as the observational reference for the model evaluation.

2.2 Model and turbulence schemes

The numerical experiments were performed with the ICOsahedral Nonhydrostatic (ICON) model version *icon-2024.01-dwd-2.0*, operated in both NWP and LES modes. ICON is a fully compressible atmospheric model jointly developed by the German

https://doi.org/10.5194/egusphere-2025-4308
Preprint. Discussion started: 16 September 2025

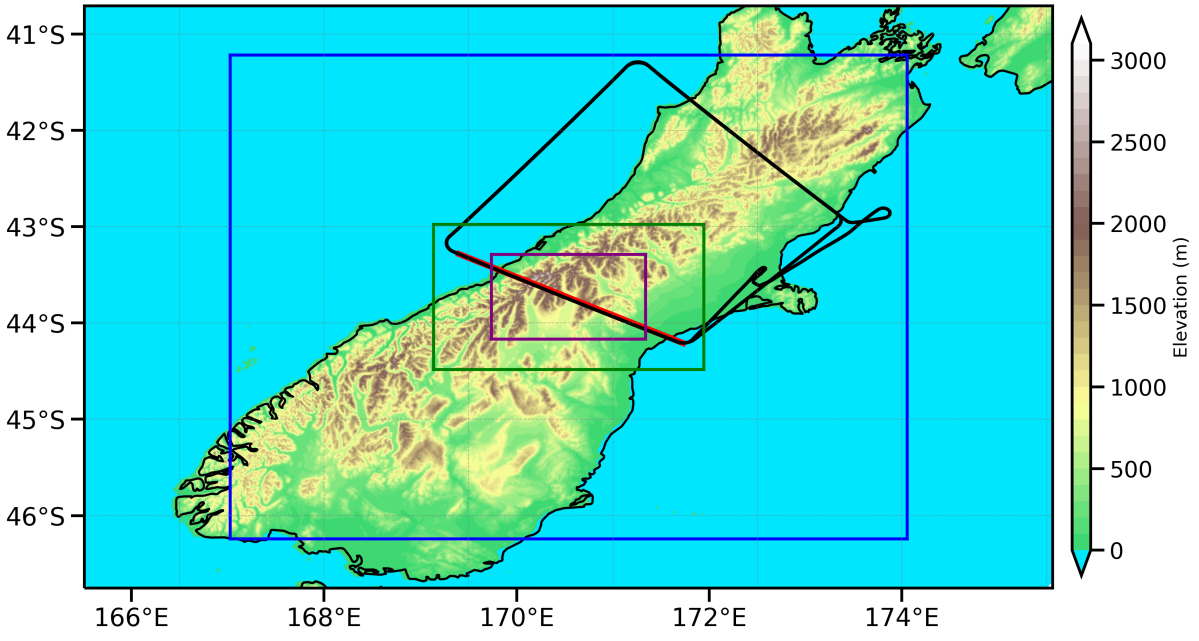

Figure 1. Orography elevation (color shading) and simulation domains for the nested ICON setup: 1 km (full region), 500 m (blue box), and 130 m for the southern flight segment (green box). The red line marks the cross-section along the flight path used for the main analysis, and the purple box indicates the averaging region for the momentum-flux profiles (Sect. 2.4). The black solid line shows the full flight path of research flight FF09 of the Falcon aircraft on 12 July 2014 (17:15–20:15 UTC) during the DEEPWAVE campaign.

Weather Service (DWD) and the Max Planck Institute for Meteorology. It employs an icosahedral-triangular grid constructed using geodesic Delaunay triangulation, a height-based vertical coordinate system, and C-grid staggering (Zängl et al., 2015). The physical parameterizations include the Tiled TERRA land surface scheme (Schulz et al., 2016), a one-moment cloud microphysics scheme with graupel (Seifert, 2008), the low-level flow blocking component of the subgrid-scale orographic drag scheme (Lott and Miller, 1997), and the ecRad radiation scheme (Hogan and Bozzo, 2018).

A central aim of this study is to assess how the simulation of mountain waves and turbulence in ICON depends on both the choice of turbulence parameterization and the model resolution. Two turbulence schemes are considered: the operational turbulent kinetic energy scheme (TKE scheme; Raschendorfer, 2001) and the more recently developed two-energy turbulence scheme (2TE scheme; Ďurán et al., 2022). The TKE scheme predicts a single turbulent kinetic energy and accounts for turbulence generation beyond vertical wind shear through additional empirical source terms for large-scale horizontal shear (HS term) and breaking subgrid-scale mountain waves (SSO term) (Goecke and Machulskaya, 2021). Its development and tuning prioritize operational NWP applications, including aviation turbulence products such as eddy dissipation rate (EDR). In contrast, the 2TE scheme predicts two prognostic turbulence energies, enabling a more flexible representation of anisotropic and stably stratified turbulence. The scheme avoids prescribed minimum diffusion coefficients, dynamically adjusts the turbulence length scale, and employs an assumed probability density function (APDF) method to represent buoyancy production.

https://doi.org/10.5194/egusphere-2025-4308
Preprint. Discussion started: 16 September 2025

Through this formulation, the 2TE scheme provides a unified framework for representing turbulence, shallow convection, and subgrid-scale cloud processes (Ďurán et al., 2018; Singh et al., 2025).

While the TKE scheme has long been used operationally and the 2TE scheme is currently under development, their performance in simulating mountain waves and associated turbulence in the UTLS has not been systematically evaluated. In addition, the sensitivity of these simulations to horizontal and vertical resolution is not well constrained, despite growing use of kilometer-scale NWP. This study therefore investigates how the two turbulence schemes, in combination with different resolutions, represent mountain-wave dynamics, turbulence characteristics, and momentum fluxes during the DEEPWAVE case. The different ICON configurations and sensitivity experiments are introduced in the following subsection.

2.3 Model configurations and simulations

Based on the two turbulence schemes described above, we carried out a set of numerical experiments with varying horizontal and vertical resolutions, complemented by nested LES and targeted sensitivity runs. The experiments are summarized in Table 1. Limited-area ICON simulations in NWP mode were conducted at horizontal grid spacings of approximately $2\,\mathrm{km}$ (I20-2TE), $1\,\mathrm{km}$ (I10-2TE, I10-TKE), and $0.5\,\mathrm{km}$ (I05-2TE). All configurations employed 137 vertical levels with spacing increasing from about $20\,\mathrm{m}$ near the surface to finer than $200\,\mathrm{m}$ up to $14\,\mathrm{km}$, a model top at $30\,\mathrm{km}$, and Rayleigh damping above $20\,\mathrm{km}$. The simulations were initialized from IFS analyses at 00:00 UTC on 12 July 2014 and integrated for $24\,\mathrm{h}$, with outputs every $30\,\mathrm{min}$ and every $5\,\mathrm{min}$ between 17:00–20:00 UTC. Among these, the I10-2TE simulation was selected as the reference case for the analysis.

A online nested LES configuration at $130\,\mathrm{m}$ (LES-S) targeted the southern flight segment. The LES was realized with four nested domains down to $130\,\mathrm{m}$, with the outermost nest run using the 2TE scheme and the inner nests employing a Smagorinsky closure.

To isolate parameterized sources of turbulence production in the TKE scheme, we additionally performed targeted sensitivity runs at $1\,\mathrm{km}$ resolution: one with only subgrid-scale orography activated (I10-TKE-SSO), one with only horizontal-shear production activated (I10-TKE-HS), and one with both terms deactivated (I10-TKE-none).

2.4 Bulk characteristics of the GW field

In addition to local characteristics, we also evaluate bulk characteristics of the simulated gravity wave field over the Southern Alps, namely the area-averaged vertical fluxes of momentum and energy induced by the waves. For this purpose, the model output on terrain-following levels was interpolated to geometric height levels, and averages were taken over the analysis domain shown in Fig. 1. The vertical fluxes of horizontal momentum are defined as

$$\overline{\rho u' w'} = \overline{\rho(u-\overline{u})(w-\overline{w})}, \qquad \overline{\rho v' w'} = \overline{\rho(v-\overline{v})(w-\overline{w})}, \tag{1}$$

where overbars denote horizontal means at a given altitude and primes the corresponding perturbations. The total flux magnitude is then given by

$$\tau = \sqrt{(\overline{\rho u' w'})^2 + (\overline{\rho v' w'})^2}. \tag{2}$$

https://doi.org/10.5194/egusphere-2025-4308
Preprint. Discussion started: 16 September 2025

Table 1. Overview of ICON model experiments used in this study. The table lists the turbulence scheme, horizontal resolution, and grid setup for each configuration, including NWP runs, nested LES, and targeted ICON-TKE sensitivity experiments. SSO refers to subgrid-scale orography, HS refers to horizontal shear, and GP denotes grid points.

Experiment	Resolution	Turbulence setup	# of GPs	Domain Size (km x km)
I20-2TE	2076 m	2TE	127466	677 x 812
I10-2TE	1038 m	2TE	502719	677 x 812
I10-TKE	1038 m	TKE, with SSO & HS	502719	677 x 812
I05-2TE	519 m	2TE	1167450	558 x 564
I01-LES-S	130 m	Smagorinsky [a]	2227352	167 x 225
I10-TKE-SSO	1038 m	TKE, with SSO	502719	677 x 812
I10-TKE-HS	1038 m	TKE, with HS	502719	677 x 812
I10-TKE-none	1038 m	TKE, no extra terms	502719	677 x 812

[a] The LES are run as an online nest consisting of four domains: 1 km, 500 m, 260 m and 130 m.

The variance of vertical velocity, $\overline{w'^2}$, follows as a special case of these definitions. Along with subgrid-scale turbulent kinetic energy, these diagnostics characterize the bulk properties of the GW field and parameterized turbulence across different resolutions and turbulence schemes. In particular, area-averaged momentum fluxes provide a measure of convergence with resolution and are an important target quantity for parameterizations in coarse-resolution models.

3 Results and Discussion

We first examine the I10-2TE simulation to establish the baseline characteristics of the wave event. This case serves as the reference for assessing the impact of resolution and turbulence parameterizations in the subsequent subsections. We chose I10-2TE as the reference because, as will be shown, the standard TKE configuration produces excessive and likely unrealistic TKE, making it less consistent as a baseline.

3.1 Reference simulation of the wave event

The reference simulation I10-2TE reproduces a distinct mountain-wave pattern over the South Island at flight time (18:00 UTC). Horizontal cross-sections of vertical velocity show alternating bands of ascent and descent downstream of the main ridge of the Southern Alps, extending from the mid-troposphere into the lower stratosphere (Fig. 2). The wave signal is most pronounced near the southern leg and south of the DEEPWAVE flight track. It is stronger in the troposphere (4 and $8\,\mathrm{km}$) than in the lower stratosphere ($11\,\mathrm{km}$), consistent with vertically propagating gravity waves. Note the dominant waves also increase in horizontal scale with altitude.

A vertical cross-section along the southern segment of the flight path at 18:00 UTC highlights the primary wave response above the topography (Fig. 3a). The transect passes near Mount Cook, New Zealand's highest mountain, at about $x = 68$ km.

https://doi.org/10.5194/egusphere-2025-4308
Preprint. Discussion started: 16 September 2025

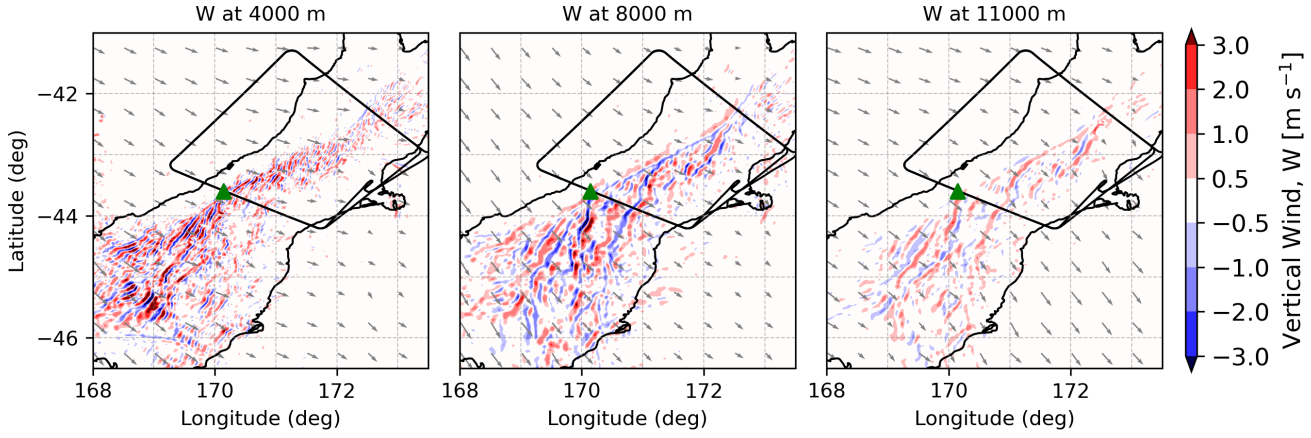

Figure 2. Horizontal cross-sections of vertical wind at heights corresponding to the lower and upper legs of the flight for the I10-2TE simulation at 18:00 UTC on 12 July 2014. Wind vectors derived from the zonal and meridional wind components are overlaid, with arrow direction indicating flow and arrow length proportional to wind speed. Vectors are plotted every 0.5° in both longitude and latitude for clarity, on a Plate Carrée projection. The full flight track is shown by the black line, and the green marker denotes the location of Mount Cook, New Zealand.

Farther southeast, at about $x = 125$ km, it crosses the Two Thumb Range, the last major ridge in this section. A strong mountain wave, with vertical velocities exceeding $3\,\mathrm{m\,s^{-1}}$, is triggered by the Mount Cook region, while a weaker wave develops above the Two Thumb Range. Both waves propagate into the lower stratosphere and are associated with leeside descent, low-level steepening of the isentropes, and the production of turbulence (subgrid-scale TKE) as seen in Fig. 3b. Significant turbulence is confined to the ABL and to regions of steep isentropes associated with lee-side flow separation. Note that non-orographic BL turbulence is weak, as expected for the early morning hours (06:00 local time).

To assess the stationarity of the simulated wave field, the same cross-section is shown one hour later at 19:00 UTC (Fig. 3c,d). While the primary waves over Mount Cook and the Two Thumb Range remain nearly unchanged, some differences emerge at smaller scales and in the UTLS region above the Two Thumb Range. Despite the near-identical wave pattern over Mount Cook, the subgrid-scale TKE is weaker at 19:00 UTC, indicating temporal evolution. In summary, the large-scale wave pattern over the Mount Cook region is quasi-stationary, whereas smaller-scale features show less stationarity.

Comparison with observations (Fig. 4) shows that the simulated wave amplitude, in terms of vertical velocity perturbations, agrees reasonably well with the lower flight leg but is strongly underestimated on the upper leg. A spatial phase mismatch between simulated and observed waves is also apparent, which is to be expected. While the simulated wave field is almost stationary — particularly for the strong wave triggered above Mount Cook — the real atmosphere is likely much less stationary due to multi-scale interactions among a spectrum of gravity waves and turbulent motions. Additional variability is also expected from temporal changes in the upstream profile. Note that the observed wave phases differ between the lower and upper flight

https://doi.org/10.5194/egusphere-2025-4308
Preprint. Discussion started: 16 September 2025

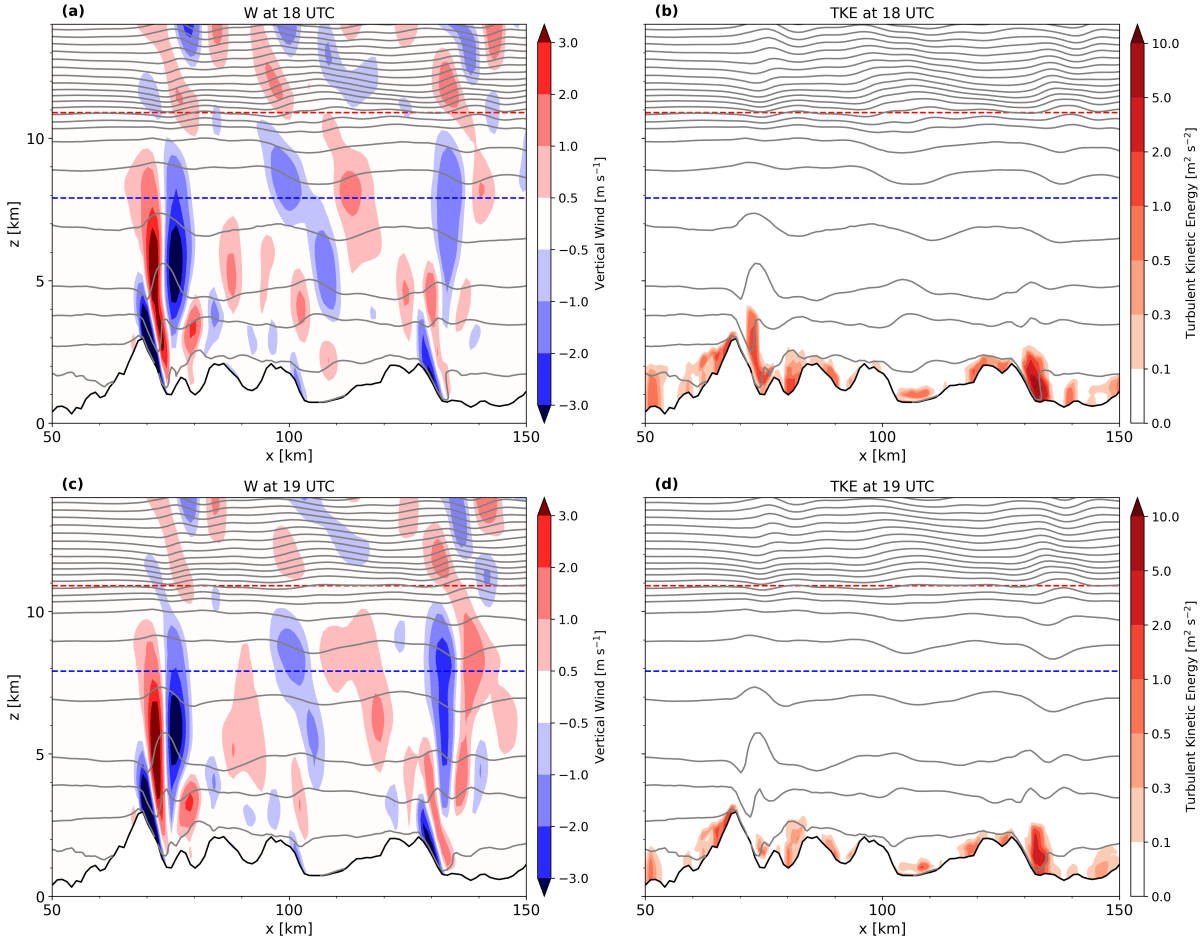

Figure 3. Vertical cross-sections of (a,c) vertical wind and (b,d) subgrid-scale turbulent kinetic energy over the southern segment of the flight track, simulated with the I10-2TE run at 18:00 UTC (a,b) and 19:00 UTC (c,d). The blue dashed line denotes the lower flight leg and the red dashed line the upper flight leg of the campaign.

https://doi.org/10.5194/egusphere-2025-4308
Preprint. Discussion started: 16 September 2025

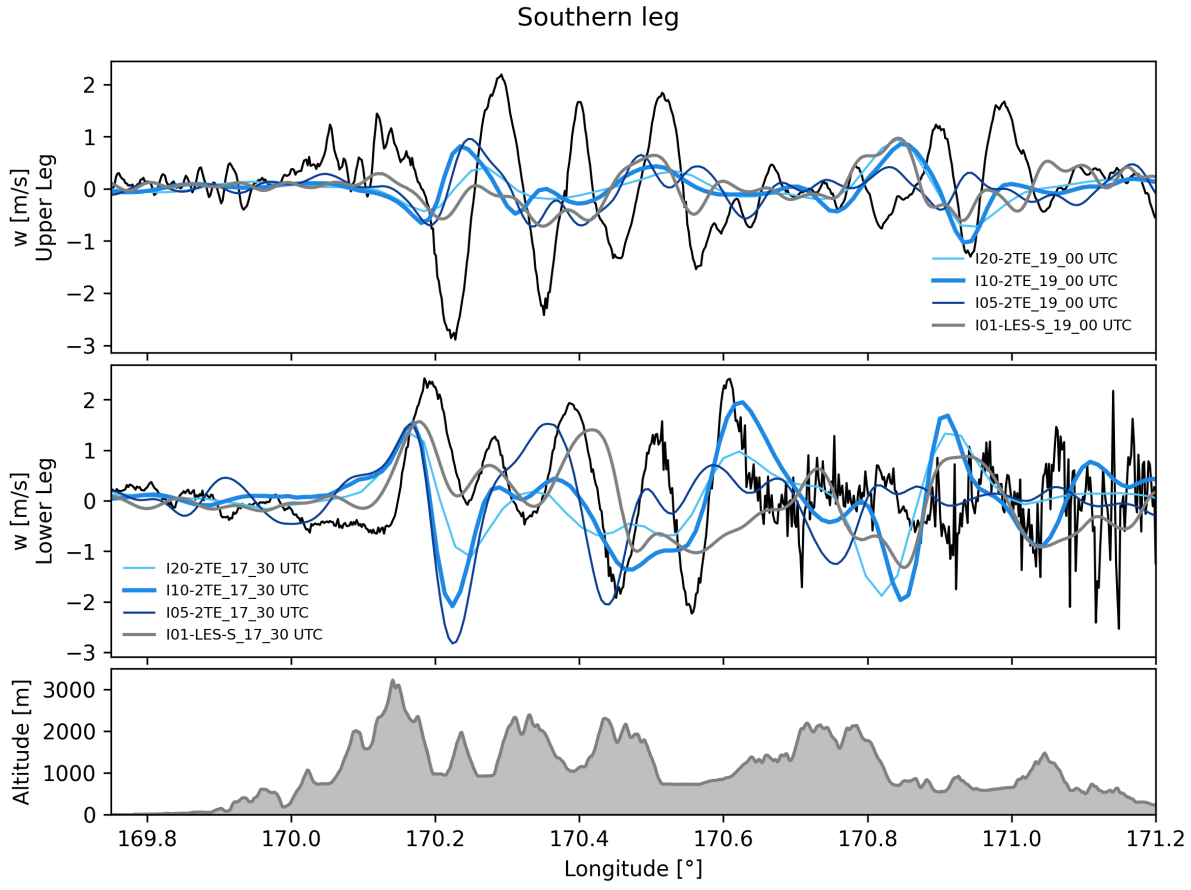

Figure 4. Comparison of vertical velocity from ICON simulations with the 2TE turbulence scheme at different horizontal resolutions and in situ observations along the southern segment of the flight track. Results are shown separately for the lower and upper flight legs, together with the underlying terrain along the cross-section. Note that 0.2° in the horizontal axis corresponds to 16 km.

legs. These differences are unlikely to reflect a vertical discontinuity; instead, they most likely result from the roughly one-hour time difference between the two legs and the non-stationary nature of the real gravity-wave field.

In summary, the reference simulation captures a strong vertically propagating mountain wave but shows no evidence of significant wave breaking or turbulence at flight altitudes associated with the dominant wave, consistent with the observations. It provides the baseline for assessing the sensitivity to model resolution and turbulence parameterization presented in the following subsections.

3.2 Sensitivity to horizontal and vertical resolution

The horizontal resolution strongly influences the simulated wave field, with substantially more wave activity at finer grid spacing (Fig. 6). At 2 km, the horizontal wavelength increases and the gravity wave appears more hydrostatic, as the model

https://doi.org/10.5194/egusphere-2025-4308
Preprint. Discussion started: 16 September 2025

cannot resolve shorter scales. This is particularly evident for the wave triggered by the Two Thumb Range. At finer resolution ($0.5\,\mathrm{km}$), the waves become more non-hydrostatic, with vertical velocity perturbations more vertically aligned. Importantly, the number of resolved waves increases as the model begins to capture shorter wavelengths. This effect is even more pronounced in the LES at $130\,\mathrm{m}$. The LES further shows that the shortest wavelengths are trapped in the layer of enhanced stability below about $5\,\mathrm{km}$, with a clear example of trapped lee waves in the lee of the Two Thumb Range. Another notable difference between the NWP simulations and the LES is the representation of the flow structure immediately downstream of the mountains (Mount Cook, an intermediate ridge at ĩ00 km, and the Two Thumb Range). In the NWP runs, the downslope flow penetrates to lower levels than in the LES, which has a significant effect on mountain-wave triggering. These differences are likely due not only to resolution, but also to the different representation of the atmospheric boundary layer and its coupling with the mountain wave (e.g. Jiang et al., 2008). For completeness, horizontal cross-sections of the flow at different resolutions are shown in Appendix A1, confirming the sensitivity of dominant gravity-wave scales to model resolution.

To gain further insight into the wave environment, upstream profiles of wind speed, potential temperature, Brunt–Väisälä frequency, and the Scorer parameter are shown in Fig. 5. The wind speed increases approximately linearly from about $10\,\mathrm{m\,s^{-1}}$ at ridge height to nearly $20\,\mathrm{m\,s^{-1}}$ just below the tropopause at $9\,\mathrm{km}$. In terms of stability, the lower troposphere (below $5\,\mathrm{km}$) is markedly more stable than the upper troposphere above. These two factors combine to produce a decrease of the Scorer parameter with height through much of the troposphere, followed by a recovery to slightly larger values in the lowermost stratosphere. The Scorer parameter profile implies a cut-off wavelength of about 5–6 km just above ridge level, increasing to roughly 12–13 km near the tropopause. This vertical structure explains the generation of trapped lee waves in the stable layer below $5\,\mathrm{km}$.

Comparison with in situ observations along the southern leg (Fig. 4) shows that the LES reproduces the observed spatial phase of the gravity wave more closely than the NWP runs, although the simulated amplitudes are too small, particularly on the upper flight leg. Among the NWP simulations, the $0.5\,\mathrm{km}$ run provides the best agreement with observed amplitudes at the lower level, but the upper-level amplitudes remain strongly underestimated. These discrepancies likely reflect, among other factors, the non-stationarity of the real wave field compared to the quasi-stationary model simulations. Note, for example, that in the $0.5\,\mathrm{km}$ run the simulated wave above Mount Cook at the altitude of the lower flight leg compares reasonably well with the observed wave at the altitude of the upper leg.

The sensitivity to vertical resolution was assessed with additional 2TE runs in which the maximum grid spacing below $14\,\mathrm{km}$ was set to $400\,\mathrm{m}$, $200\,\mathrm{m}$, and $100\,\mathrm{m}$, respectively. The coarsest grid ($400\,\mathrm{m}$) shows clear differences from the reference run, particularly in the stratosphere, whereas the $200\,\mathrm{m}$ and $100\,\mathrm{m}$ results are very similar, indicating near-convergence at $200\,\mathrm{m}$ (not shown). This finding motivated the choice of a maximum vertical spacing of $200\,\mathrm{m}$ as the default in the NWP setup used here.

https://doi.org/10.5194/egusphere-2025-4308
Preprint. Discussion started: 16 September 2025

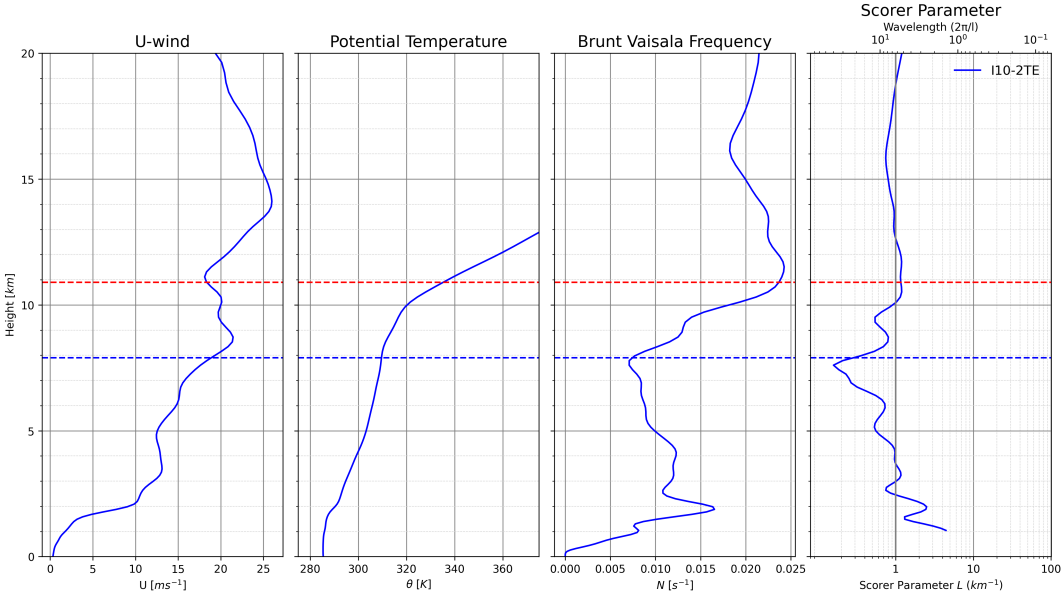

Figure 5. Upstream profiles of wind speed parallel to the southern flight leg (u), potential temperature (θ), Brunt–Väisälä frequency (N), and Scorer parameter (L) from the I10-2TE simulation. Profiles are taken 10 km upstream of the start of the red transect line in Fig. 1, at 18:00 UTC (flight time). All variables are smoothed in the vertical using a Gaussian filter with a standard deviation of 1.5 vertical grid points.

3.3 Sensitivity to turbulence parameterization

3.3.1 Comparison of the two turbulence schemes

At 1 km resolution, the two turbulence schemes produce rather similar wave patterns, particularly for the wave field above Mount Cook (Figs.7a,c), as also seen in the horizontal cross-sections (Fig.A2). In contrast, the simulated turbulent kinetic energy differs markedly between the schemes (Figs. 7b,d). The TKE scheme produces substantially higher TKE values throughout the wave field, whereas the 2TE scheme confines turbulence mainly to the ABL and the strongest low-level mountain waves. The elevated TKE values above the ABL and outside regions of strong gravity-wave activity appear questionable and warrant further investigation. A key difference between the two schemes is the inclusion of additional empirical source terms in the TKE scheme. This motivated further experiments to isolate the impact of these terms.

3.3.2 Effect of optional TKE source terms in the TKE scheme

Sensitivity experiments with individual source terms switched off are shown in Fig. 8. These targeted experiments allow us to disentangle the effects of the horizontal shear and subgrid-scale orography terms. The simulated wave structures respond to these modifications: vertical velocity patterns change, particularly in I10-TKE-HS, where only the horizontal shear term is activated and the SSO term is deactivated. Even more striking are the differences in the TKE fields. In I10-TKE and I10-TKE-

https://doi.org/10.5194/egusphere-2025-4308
Preprint. Discussion started: 16 September 2025

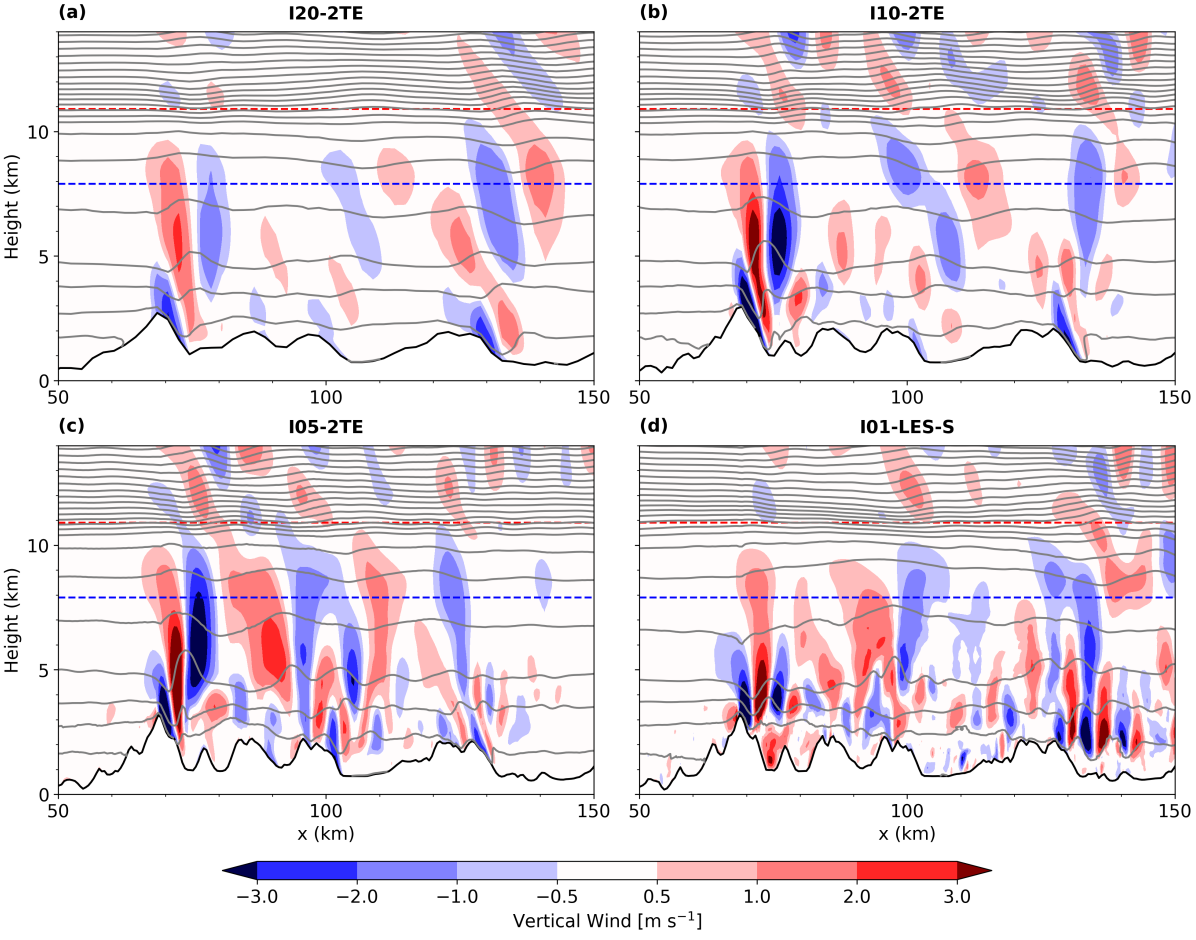

Figure 6. Comparison of vertical velocity on 12 July 2014 at 18:00 UTC along the southern flight path transect (red line in Fig. 1, from 50 to 150 km) for 2TE simulations at different horizontal resolutions: (a) 2 km, (b) 1 km, (c) 500 m, and (d) 130 m.

HS, which both include the horizontal shear term, substantial TKE appears not only in the ABL and low-level flow-separation regions but also in patches throughout the troposphere, with weaker pockets even extending into the lower stratosphere. In contrast, I10-TKE-SSO and I10-TKE-none, which exclude the horizontal shear term, produce TKE distributions more similar to those obtained with the 2TE scheme. The occurrence of large TKE values in regions without strong wave activity appears unrealistic, suggesting that the empirical parameterization of the horizontal shear term is not suitable for high-resolution simulations. This finding is consistent with Bramberger et al. (2020), who showed that the Graphical Turbulence Guidance tool, which uses a similar empirical formulation, overpredicted turbulence magnitude over a large area during a breaking mountain-wave event over Iceland. The SSO term, in contrast, may improve realism: in I10-TKE-SSO the low-level wave structure in the lee of major mountains is closer to the LES than in the other simulations and partly compensates for the effects of the horizontal shear term, bringing the standard TKE setup (I10-TKE) closer to results obtained with the 2TE scheme.

https://doi.org/10.5194/egusphere-2025-4308
Preprint. Discussion started: 16 September 2025

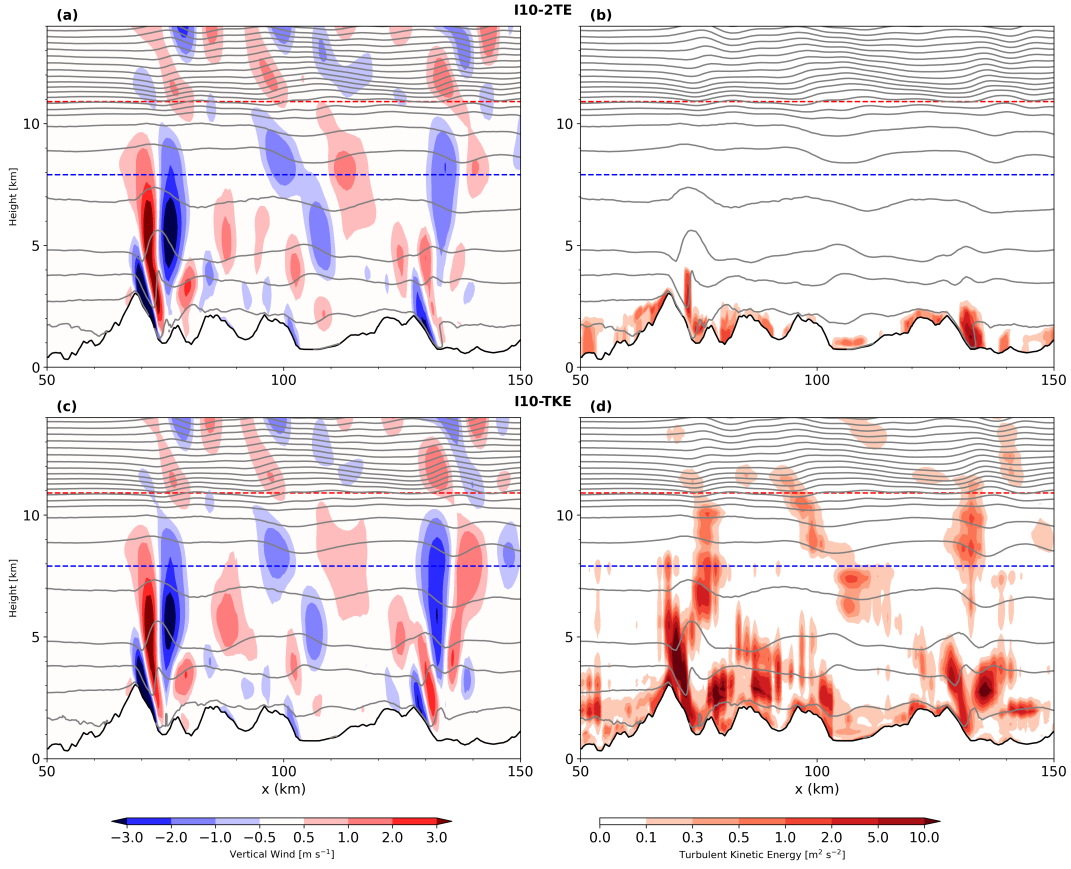

Figure 7. Comparison of vertical velocity on 12 July 2014 at 18:00 UTC along the southern flight path transect (red line in Fig. 1, from 50 to 150 km) for ICON simulations with (a, b) the 2TE scheme and (c, d) the TKE scheme, both at 1 km horizontal resolution.

3.4 Bulk properties of the GW field

3.4.1 Vertical velocity variance and SGS-TKE

Domain-averaged profiles of resolved vertical velocity variance ($\overline{w'^2}$) and SGS-TKE highlight important differences in how resolution and turbulence schemes represent small-scale energy (Fig. 9). Among the 2TE simulations, the 0.5 km run performs particularly well. Its variance profile is in good agreement with the LES in the lower troposphere, demonstrating that fine-scale vertical motions are effectively captured at this resolution. In contrast, coarser runs at 1 km and 2 km systematically underestimate the variance, with the discrepancy growing toward the surface where the flow interacts more strongly with the orography. This highlights that quasi-LES resolutions on the order of a few hundred meters are required to reproduce the vertical distribution of wave-induced variance for this mountain wave event.

https://doi.org/10.5194/egusphere-2025-4308
Preprint. Discussion started: 16 September 2025

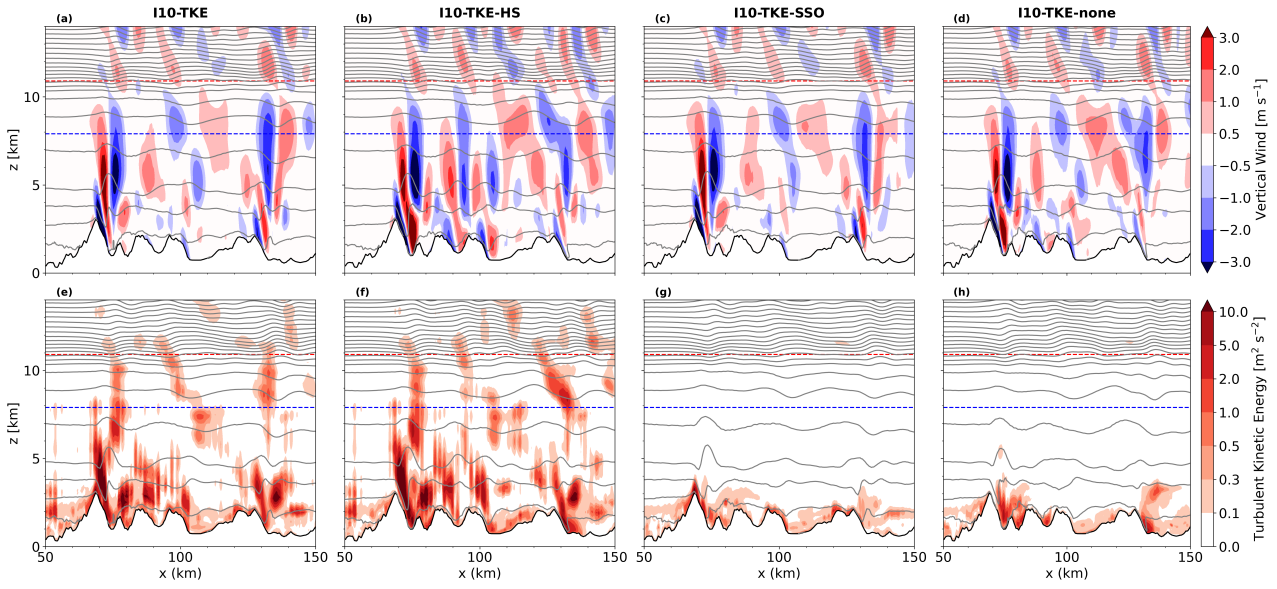

Figure 8. Comparison of vertical cross-sections of vertical velocity and turbulent kinetic energy along the southern flight path transect (red line in Fig. 1, from 50 to 150 km) for ICON simulations with the TKE scheme: (a, b) both horizontal shear (HS) and subgrid-scale orography (SSO) active, (c, d) SSO deactivated, (e, f) horizontal shear deactivated, and (g, h) both HS and SSO deactivated.

At $1\,\mathrm{km}$ resolution, the resolved variances ($\overline{w'^2}$) are broadly similar between the two turbulence schemes, but the SGS-TKE fields differ substantially. Simulations with the TKE scheme generate larger SGS-TKE values than those with the 2TE scheme, particularly when the horizontal shear term is active. These inflated values contrast with the more realistic profiles from the 2TE simulations. Together, these findings emphasize that, while resolved variances converge toward LES at sufficiently fine resolution, the representation of SGS-TKE remains highly sensitive to the choice of turbulence formulation.

3.4.2 Wave momentum fluxes

Domain-averaged profiles of vertical momentum flux illustrate how resolution and turbulence schemes influence the representation of wave-induced transport (Fig. 10). In the 2TE simulations, the $0.5\,\mathrm{km}$ run converges toward the LES, while the $2\,\mathrm{km}$ run shows reduced fluxes, especially in the lower troposphere. The $1\,\mathrm{km}$ simulation lies between these two, indicating that horizontal grid spacings of about $1\,\mathrm{km}$ or finer are needed for near-converged momentum flux profiles.

At $1\,\mathrm{km}$ resolution, the TKE and 2TE schemes produce very similar vertical structures of momentum flux despite their large differences in SGS-TKE. This suggests that the empirical horizontal shear term in the TKE scheme inflates the subgrid TKE but has little influence on the bulk momentum flux. Overall, the results highlight that area-averaged momentum flux converges more rapidly with resolution than local turbulence diagnostics, making momentum flux a more robust diagnostic for evaluating mountain-wave simulations.

https://doi.org/10.5194/egusphere-2025-4308
Preprint. Discussion started: 16 September 2025

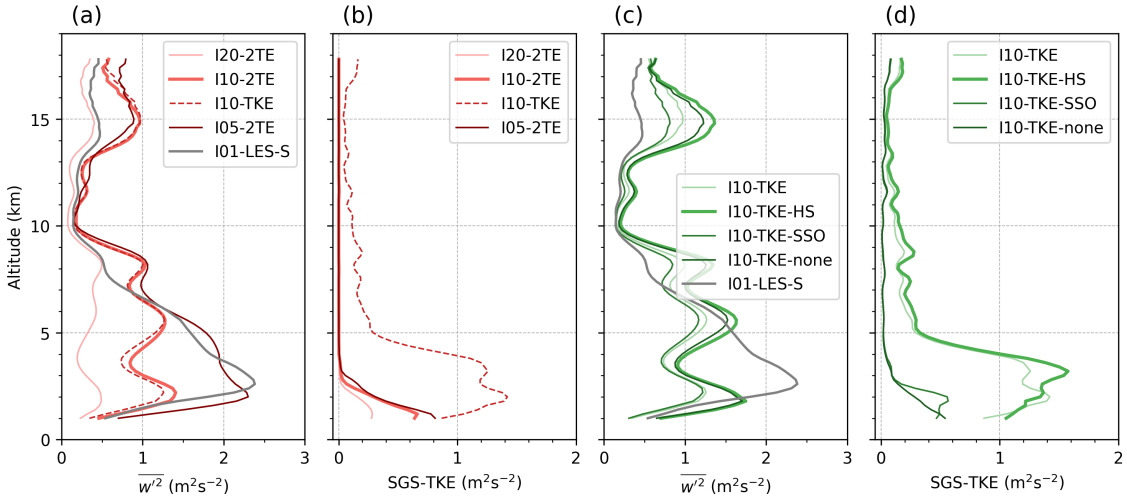

Figure 9. Profiles of resolved vertical velocity variance ($\overline{w'^2}$) and subgrid-scale turbulent kinetic energy (SGS-TKE), averaged over the analysis domain shown in Fig. 1, for (a) different horizontal resolutions with the 2TE scheme and I10-TKE and (b) different configurations of the TKE scheme.

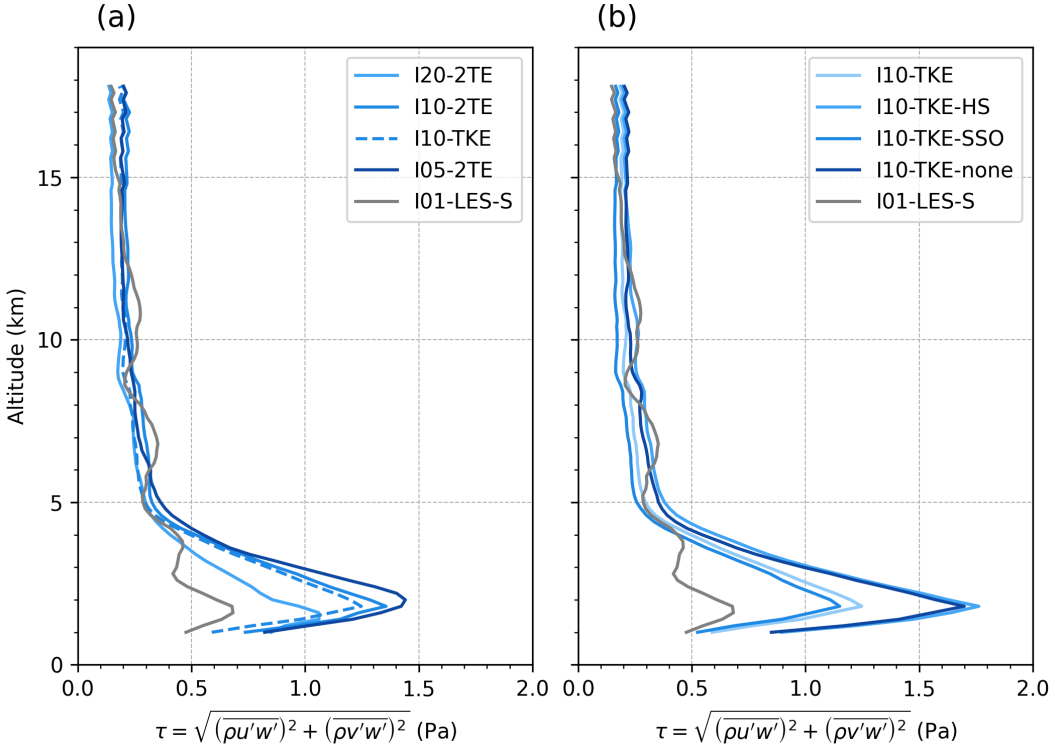

Figure 10. Vertical profiles of domain-averaged momentum flux for (a) 2TE simulations at different horizontal resolutions and (b) TKE simulations at 1 km resolution on 12 July 2014 at 18:00 UTC. Fluxes are calculated within the subdomain shown in Fig. 1 after interpolation to regular vertical levels with 200 m spacing.

https://doi.org/10.5194/egusphere-2025-4308
Preprint. Discussion started: 16 September 2025

4 Conclusions

This study investigated the simulation of mountain waves with the ICON model, focusing on the influence of horizontal and vertical resolution and the representation of turbulence through different parameterization schemes. We examined the performance of the newly implemented two-energy scheme (2TE scheme) in reproducing mountain-wave structures and associated turbulence during a case from the DEEPWAVE campaign over New Zealand on 12 July 2014. Model simulations were compared with high-frequency aircraft observations and nested LES runs for detailed visual and statistical evaluation.

Our results demonstrated that both vertical and horizontal resolutions play a critical role in accurately capturing the structure and behavior of mountain waves. We found that a vertical grid spacing of less than $200\,\mathrm{m}$ is necessary to adequately resolve the wave field in the UTLS region. Insufficient vertical resolution damps the wave amplitude, leading to underestimation of wave strength. For horizontal resolution, simulations at $0.5\,\mathrm{km}$ approached the LES in terms of wavelength, while coarser runs ($1\,\mathrm{km}$–$2\,\mathrm{km}$) underestimated the number and detail of shorter waves. Differences between NWP and LES simulations also point to the importance of how the ABL is represented, since ABL coupling affects lee-side flow separation, and thus the triggering of mountain waves.

A central component of this study was the evaluation of the 2TE turbulence scheme compared against the operational TKE scheme. Both schemes produced similar mountain-wave structures and comparable domain-averaged profiles of momentum flux, which are essential for capturing the vertical transport of energy and momentum. However, they diverged strongly in their representation of SGS-TKE. While the 2TE scheme yielded smooth, physically consistent fields, the TKE scheme exhibited elevated and spatially erratic SGS-TKE, particularly when the horizontal shear term was active. These unrealistic values are attributed to the empirical parameterization of horizontal shear in the TKE scheme, consistent with findings by Bramberger et al. (2020), who documented similar overpredictions in turbulence guidance products.

Hence, our findings suggest that careful reevaluation of turbulence parameterizations is required when using high-resolution NWP models in mountainous terrain. For kilometer-scale resolutions, model setups should consider disabling or tuning the horizontal shear and SSO terms in the TKE scheme to avoid spurious SGS-TKE production. Alternatively, schemes such as 2TE provide a promising framework for turbulence representation at these scales.

The results have important implications for the configuration of high-resolution regional weather models and for advancing the understanding of terrain-induced gravity waves and associated turbulent processes. Future work will extend this analysis to additional DEEPWAVE cases and other campaigns to test the robustness of these conclusions. A further priority is coupling the 2TE scheme with gravity-wave parameterizations to bridge explicitly resolved and parameterized wave–turbulence interactions, particularly in global and climate modeling frameworks.

https://doi.org/10.5194/egusphere-2025-4308
Preprint. Discussion started: 16 September 2025

Appendix A

A0.1 Horizontal cross sections

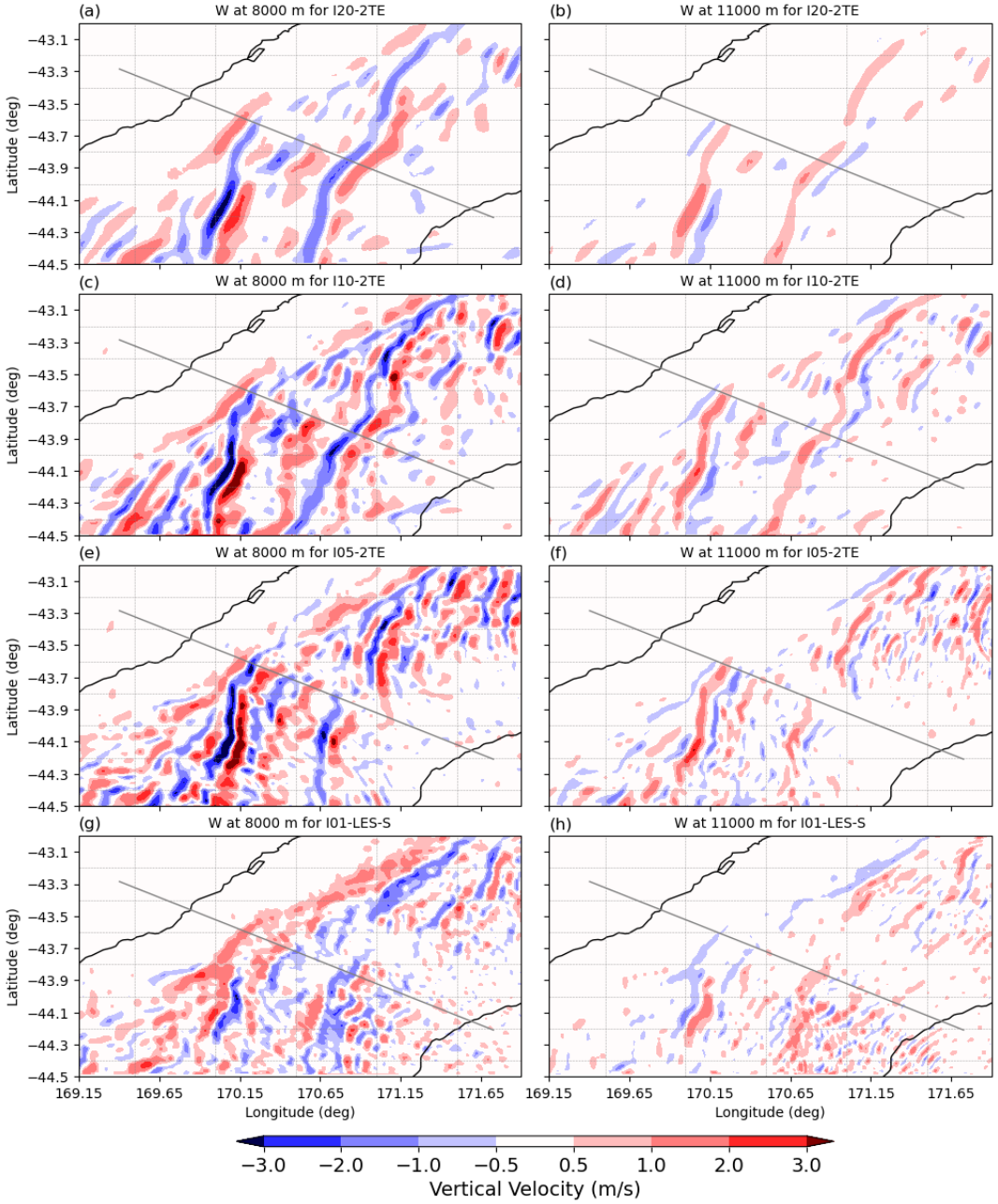

Figure A1. Horizontal cross-sections of vertical velocity at 8000 m and 11 000 m, corresponding to the lower and upper flight legs, for ICON simulations with the 2TE turbulence scheme at different horizontal resolutions, together with the LES. The comparison highlights how finer resolution captures shorter-scale wave features and approaches the LES in reproducing the observed wave structures.

https://doi.org/10.5194/egusphere-2025-4308
Preprint. Discussion started: 16 September 2025

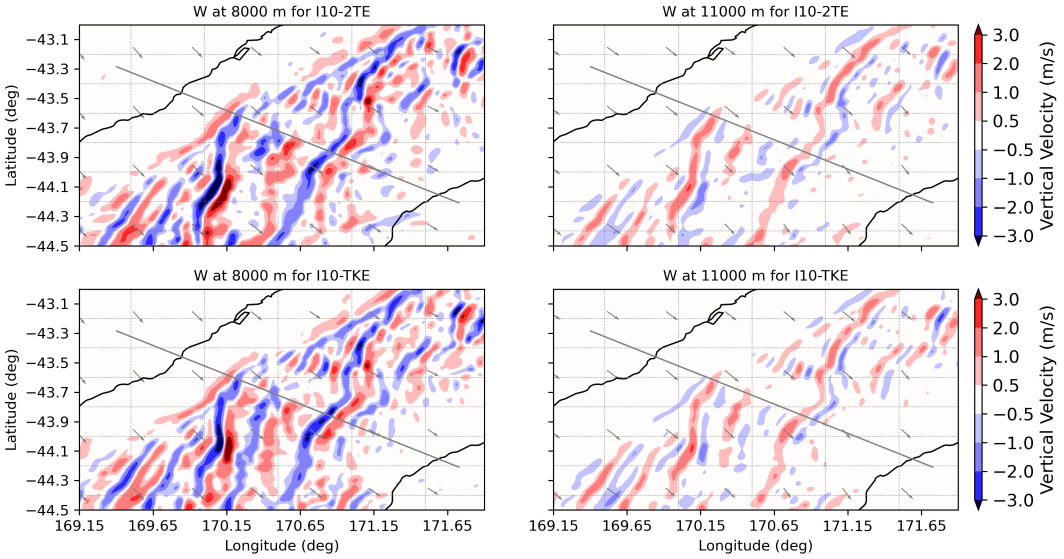

Figure A2. Horizontal cross-sections of vertical velocity at 8000 m and 11 000 m, corresponding to the lower and upper flight legs, for ICON simulations I10-2TE and I10-TKE. The two simulations produce broadly similar wave structures, indicating that differences between the schemes are primarily reflected in the subgrid-scale turbulence fields rather than in the resolved vertical velocity patterns.

Code and data availability. The airborne measurement data from the DEEPWAVE campaign are available through the HALO database (https://doi.org/10.17616/R39Q0T; HALO-DB, 2022). We thank Hans-Christoph Lachnitt for providing the post-processed data in a convenient format. The ICON model is distributed under an open-source BSD-3C license (https://www.icon-model.org) and is publicly available at https://gitlab.dkrz.de/icon/icon-model/-/releases/icon-2025.04-1-public (GitLab, 2025). The ICON-2TE implementation is included in the ICON source code and can be made available on request. The simulation output, processing resources, and analysis scripts used to generate the figures in this paper are available from the corresponding author upon request.

Author contributions. RS: conceptualization, model implementation and simulations, data curation, formal analysis, visualization, writing — original draft, and writing — review and editing. JS: conceptualization, methodology, model scheme development, funding acquisition, project administration, supervision, software, and writing — review and editing.

Competing interests. The authors have declared that there are no competing interests.

https://doi.org/10.5194/egusphere-2025-4308
Preprint. Discussion started: 16 September 2025

Acknowledgements. The authors thank the German Research Foundation (DFG) for financial support through CRC 301 TPChange (Project-ID 428312742, sub-projects B06 “Impact of small-scale dynamics on UTLS transport and mixing” and Z03 “Joint model development”). This work used resources of the Deutsches Klimarechenzentrum (DKRZ), granted by its Scientific Steering Committee (WLA) under project ID bb1096. We thank Dr. Hans-Christoph Lachnitt and Dr. Peter Hoor for providing the processed observational data for the case study from the HALO database, and Dr. Tobias Goecke for constructive discussions.

https://doi.org/10.5194/egusphere-2025-4308
Preprint. Discussion started: 16 September 2025

References

Achatz, U., Alexander, M. J., Becker, E., Chun, H.-Y., Holt, L., Plougonven, R., Polichtchouk, I., Sato, K., Sheshadri, A., Stephan, C. C., Niekerk, A. V., and Wright, C. J.: Atmospheric Gravity Waves: Processes and Parameterization, JOURNAL OF THE ATMOSPHERIC SCIENCES, 81, 2024.

Arbor, A.: A Numerical Study of Gravity Wave Breaking and Impacts on Turbulence and Mean State, JOURNAL OF THE ATMOSPHERIC SCIENCES, 56, 1999.

Bougeault, P., Jansa, A., Attié, J.-L., Beau, I., Benesch, B., Benoit, R., Bessemoulin, P., Caccia, J., Campins, J., Carissimo, B., Champeaux, J.-L., Crochet, M., Druilhet, A., Durand, P., El Khalfi, A., Flamant, P., A, G., Georgelin, M., Hoinka, K., and Tannhauser, D.: The atmospheric momentum budget over a major mountain range: First results of the PYREX field program, Annales Geophysicae, 11, 395–418, 1993.

Bougeault, P., Binder, P., Buzzi, A., Dirks, R., Houze, R., Kuettner, J., Smith, R. B., Steinacker, R., and VoIkert, H.: The MAP Special Observing Period, Bulletin of the American Meteorological Society, 82, 433–462, https://doi.org/10.1175/1520-0477(2001)082<0433:TMSOP>2.3.CO;2, publisher: American Meteorological Society Section: Bulletin of the American Meteorological Society, 2001.

Bramberger, M., Ewald, F., and Sharman, R.: Mountain-Wave Turbulence Encounter of the Research Aircraft HALO above Iceland, JOURNAL OF APPLIED METEOROLOGY AND CLIMATOLOGY, 59, 2020.

Durran, D.: MOUNTAIN METEOROLOGY Lee Waves and Mountain Waves, in: Encyclopedia of Atmospheric Sciences, edited by Gerald R. North, John Pyle, and Fuqing Zhang, vol. 4, pp. 95–102, Academic Press, 2nd edn., ISBN 978-0-12-382225-3, https://doi.org/10.1016/B978-0-12-382225-3.00202-4, https://www.sciencedirect.com/science/article/pii/B9780123822253002024, 2015.

Dörnbrack, A., Gerz, T., and Schumann, U.: Turbulent breaking of overturning gravity waves below a critical level, Applied Scientific Research, 54, 163–195, https://doi.org/10.1007/BF00849114, 1995.

Fritts, D. C. and Alexander, M. J.: Gravity wave dynamics and effects in the middle atmosphere, Reviews of Geophysics, 41, 2001RG000 106, https://doi.org/10.1029/2001RG000106, 2003.

Fritts, D. C., Smith, R. B., Taylor, M. J., Doyle, J. D., Eckermann, S. D., Dörnbrack, A., Rapp, M., Williams, B. P., Pautet, P.-D., Bossert, K., Criddle, N. R., Reynolds, C. A., Reinecke, P. A., Uddstrom, M., Revell, M. J., Turner, R., Kaifler, B., Wagner, J. S., Mixa, T., Kruse, C. G., Nugent, A. D., Watson, C. D., Gisinger, S., Smith, S. M., Lieberman, R. S., Laughman, B., Moore, J. J., Brown, W. O., Haggerty, J. A., Rockwell, A., Stossmeister, G. J., Williams, S. F., Hernandez, G., Murphy, D. J., Klekociuk, A. R., Reid, I. M., and Ma, J.: The Deep Propagating Gravity Wave Experiment (DEEPWAVE): An Airborne and Ground-Based Exploration of Gravity Wave Propagation and Effects from Their Sources throughout the Lower and Middle Atmosphere, Bulletin of the American Meteorological Society, 97, 425–453, https://doi.org/10.1175/BAMS-D-14-00269.1, 2016.

Fritts, D. C., Lund, T. S., Wan, K., and Liu, H.-L.: Numerical Simulation of Mountain Waves over the Southern Andes. Part II: Momentum Fluxes and Wave–Mean-Flow Interactions, Journal of the Atmospheric Sciences, 78, 3069–3088, https://doi.org/10.1175/JAS-D-20-0207.1, 2021.

Fritts, D. C., Lund, A. C., Lund, T. S., and Yudin, V.: Impacts of Limited Model Resolution on the Representation of Mountain Wave and Secondary Wave Dynamics in Local and Global Models: 2. Mountain Wave and Secondary Wave Evolutions in the Thermosphere, Journal of Geophysical Research: Atmospheres, 127, e2021JD036 035, https://doi.org/10.1029/2021JD036035, 2022.

Goecke, T. and Machulskaya, E.: Aviation Turbulence Forecasting at DWD with ICON: Methodology, Case Studies, and Verification, Monthly Weather Review, 149, 2115–2130, https://doi.org/10.1175/MWR-D-19-0383.1, 2021.

https://doi.org/10.5194/egusphere-2025-4308
Preprint. Discussion started: 16 September 2025

Grubišić, V. and Lewis, J. M.: SIERRA WAVE PROJECT REVISITED: 50 Years Later, Bulletin of the American Meteorological Society, 85, 1127–1142, https://doi.org/10.1175/BAMS-85-8-1127, 2004.

Grubišić, V., Doyle, J. D., Kuettner, J., Mobbs, S., Smith, R. B., Whiteman, C. D., Dirks, R., Czyzyk, S., Cohn, S. A., Vosper, S., Weissmann, M., Haimov, S., De Wekker, S. F. J., Pan, L. L., and Chow, F. K.: THE TERRAIN-INDUCED ROTOR EXPERIMENT: A Field Campaign Overview Including Observational Highlights, Bulletin of the American Meteorological Society, 89, 1513–1534, https://doi.org/10.1175/2008BAMS2487.1, 2008.

Heale, C. J., Bossert, K., and Vadas, S. L.: 3D Numerical Simulation of Secondary Wave Generation From Mountain Wave Breaking Over Europe, Journal of Geophysical Research: Atmospheres, 127, https://doi.org/10.1029/2021JD035413, e2021JD035413, 2022.

Hogan, R. J. and Bozzo, A.: A Flexible and Efficient Radiation Scheme for the ECMWF Model, Journal of Advances in Modeling Earth Systems, 10, 1990–2008, https://doi.org/10.1029/2018MS001364, 2018.

Holt, L. A., Alexander, M. J., Coy, L., Liu, C., Molod, A., Putman, W., and Pawson, S.: An evaluation of gravity waves and gravity wave sources in the Southern Hemisphere in a 7 km global climate simulation, Quarterly Journal of the Royal Meteorological Society, 143:, 2481–2495, https://doi.org/10.1002/qj.3101, 2017.

Jackson, D. R., Gadian, A., Hindley, N. P., Hoffmann, L., Hughes, J., King, J., Moffat-Griffin, T., Moss, A. C., Ross, A. N., Vosper, S. B., Wright, C. J., and Mitchell, N. J.: The South Georgia Wave Experiment: A Means for Improved Analysis of Gravity Waves and Low-Level Wind Impacts Generated from Mountainous Islands, Bulletin of the American Meteorological Society, 99, 1027–1040, https://doi.org/10.1175/BAMS-D-16-0151.1, 2018.

Jiang, Q., Smith, R. B., and Doyle, J. D.: Impact of the Atmospheric Boundary Layer on Mountain Waves, Journal of the Atmospheric Sciences, 65, 592–608, https://doi.org/10.1175/2007JAS2376.1, 2008.

Kim, S.-H., Kim, J.-H., Chun, H.-Y., and Sharman, R. D.: Global response of upper-level aviation turbulence from various sources to climate change, npj Climate and Atmospheric Science, 6, 92, https://doi.org/10.1038/s41612-023-00421-3, 2023.

Kleeorin, N., Rogachevskii, I., Soustova, I. A., Troitskaya, Y. I., Ermakova, O. S., and Zilitinkevich, S.: Internal gravity waves in the energy and flux budget turbulence-closure theory for shear-free stably stratified flows, Physical Review E, 99, 063 106, https://doi.org/10.1103/PhysRevE.99.063106, 2019.

Kuettner, J. P. and O'Neill, T. H. R.: ALPEX The GARP Mountain Subprogram, Bulletin of the American Meteorological Society, 62, 793–805, https://doi.org/10.1175/1520-0477-62.6.793, 1981.

Lachnitt, H.-C., Hoor, P., Kunkel, D., Bramberger, M., Dörnbrack, A., Müller, S., Reutter, P., Giez, A., Kaluza, T., and Rapp, M.: Gravity-wave-induced cross-isentropic mixing: a DEEPWAVE case study, Atmospheric Chemistry and Physics, 23, 355–373, https://doi.org/10.5194/acp-23-355-2023, 2023.

Lott, F. and Miller, M. J.: A new subgrid-scale orographic drag parametrization: Its formulation and testing, Quarterly Journal of the Royal Meteorological Society, 123, 101–127, https://doi.org/10.1002/qj.49712353704, 1997.

Lund, T. S., Fritts, D. C., Wan, K., Laughman, B., and Liu, H.-L.: Numerical Simulation of Mountain Waves over the Southern Andes. Part I: Mountain Wave and Secondary Wave Character, Evolutions, and Breaking, Journal of the Atmospheric Sciences, 77, 4337–4356, https://doi.org/10.1175/JAS-D-19-0356.1, 2020.

Mahalov, A.: Turbulence and Waves in the Upper Troposphere and Lower Stratosphere, in: Aviation Turbulence, edited by Sharman, R. and Lane, T., pp. 407–424, Springer International Publishing, Cham, ISBN 978-3-319-23629-2 978-3-319-23630-8, https://doi.org/10.1007/978-3-319-23630-8_20, 2016.

https://doi.org/10.5194/egusphere-2025-4308
Preprint. Discussion started: 16 September 2025

Mirza, A. K., Dacre, H. F., and Lo, C. H. B.: A case study analysis of the impact of a new free tropospheric turbulence scheme on the dispersion of an atmospheric tracer, Quarterly Journal of the Royal Meteorological Society, 150, 1907–1925, https://doi.org/10.1002/qj.4681, 2024.

Muños-Esparza, D., Sharman, R. D., and Trier, S. B.: On the Consequences of PBL Scheme Diffusion on UTLS Wave and Turbulence Representation in High-Resolution NWP Models, MONTHLY WEATHER REVIEW, 148, 2020.

Paoli, R., Thouron, O., Escobar, J., Picot, J., and Cariolle, D.: High-resolution large-eddy simulations of stably stratified flows: application to subkilometer-scale turbulence in the upper troposphere–lower stratosphere, Atmospheric Chemistry and Physics, 14, 5037–5055, https://doi.org/10.5194/acp-14-5037-2014, 2014.

Plougonven, R., de la Cámara, A., Hertzog, A., and Lott, F.: How does knowledge of atmospheric gravity waves guide their parameterizations?, Quarterly Journal of the Royal Meteorological Society, 146, 1529–1543, https://doi.org/10.1002/qj.3732, _eprint: https://onlinelibrary.wiley.com/doi/pdf/10.1002/qj.3732, 2020.

Rapp, M., Kaifler, B., Dörnbrack, A., Gisinger, S., Mixa, T., Reichert, R., Kaifler, N., Knobloch, S., Eckert, R., Wildmann, N., Giez, A., Krasauskas, L., Preusse, P., Geldenhuys, M., Riese, M., Woiwode, W., Friedl-Vallon, F., Sinnhuber, B.-M., Torre, A. D. L., Alexander, P., Hormaechea, J. L., Janches, D., Garhammer, M., Chau, J. L., Conte, J. F., Hoor, P., and Engel, A.: SOUTHTRAC-GW: An Airborne Field Campaign to Explore Gravity Wave Dynamics at the World's Strongest Hotspot, Bulletin of the American Meteorological Society, 102, E871–E893, https://doi.org/10.1175/BAMS-D-20-0034.1, 2021.

Raschendorfer, M.: The new turbulence parameterization of LM, COSMO Newsletter, 1, 89–97, http://www.cosmo-model.org, 2001.

Ren, D. and Lynch, M. J.: Changes in Global Aviation Turbulence in the Remote Sensing Era (1979–2018), Remote Sensing, 16, https://doi.org/10.3390/rs16112038, 2024.

Riese, M., Ploeger, F., Rap, A., Vogel, B., Konopka, P., Dameris, M., and Forster, P.: Impact of uncertainties in atmospheric mixing on simulated UTLS composition and related radiative effects, Journal of Geophysical Research: Atmospheres, 117, 2012JD017 751, https://doi.org/10.1029/2012JD017751, 2012.

Rodriguez Imazio, P., Mininni, P. D., Godoy, A., Rivaben, N., and Dörnbrack, A.: Not All Clear Air Turbulence Is Kolmogorov—The Fine-Scale Nature of Atmospheric Turbulence, Journal of Geophysical Research: Atmospheres, 128, e2022JD037 491, https://doi.org/10.1029/2022JD037491, 2023.

Rogel, L., Ricard, D., Bazile, E., and Sandu, I.: Effects of subgrid-scale turbulence parametrization on the representation of clear-air turbulence using kilometre- to hectometre-scale numerical simulations, Quarterly Journal of the Royal Meteorological Society, 149, 3301–3322, https://doi.org/10.1002/qj.4557, 2023.

Schäfler, A., Craig, G., Wernli, H., Arbogast, P., Doyle, J. D., McTaggart-Cowan, R., Methven, J., Rivière, G., Ament, F., Boettcher, M., Bramberger, M., Cazenave, Q., Cotton, R., Crewell, S., Delanoë, J., Dörnbrack, A., Ehrlich, A., Ewald, F., Fix, A., Grams, C. M., Gray, S. L., Grob, H., Groß, S., Hagen, M., Harvey, B., Hirsch, L., Jacob, M., Kölling, T., Konow, H., Lemmerz, C., Lux, O., Magnusson, L., Mayer, B., Mech, M., Moore, R., Pelon, J., Quinting, J., Rahm, S., Rapp, M., Rautenhaus, M., Reitebuch, O., Reynolds, C. A., Sodemann, H., Spengler, T., Vaughan, G., Wendisch, M., Wirth, M., Witschas, B., Wolf, K., and Zinner, T.: The North Atlantic Waveguide and Downstream Impact Experiment, Bulletin of the American Meteorological Society, 99, 1607–1637, https://doi.org/10.1175/BAMS-D-17-0003.1, 2018.

Scherllin-Pirscher, B., Steiner, A. K., Anthes, R. A., Alexander, M. J., Alexander, S. P., Biondi, R., Birner, T., Kim, J., Randel, W. J., Son, S.-W., Tsuda, T., and Zeng, Z.: Tropical Temperature Variability in the UTLS: New Insights from GPS Radio Occultation Observations, Journal of Climate, 34, 2813–2838, https://doi.org/10.1175/JCLI-D-20-0385.1, 2021.

https://doi.org/10.5194/egusphere-2025-4308
Preprint. Discussion started: 16 September 2025

Schneider, A., Wagner, J., Faber, J., Gerding, M., and Lübken, F.-J.: Case study of wave breaking with high-resolution turbulence measurements with LITOS and WRF simulations, Atmospheric Chemistry and Physics, 2017.

Schulz, J.-P., Vogel, G., Becker, C., Kothe, S., Rummel, U., and Ahrens, B.: Evaluation of the ground heat flux simulated by a multilayer land surface scheme using high-quality observations at grass land and bare soil, Meteorologische Zeitschrift, 25, 607–620, https://doi.org/10.1127/metz/2016/0537, 2016.

Schäfler, A., Sprenger, M., Wernli, H., Fix, A., and Wirth, M.: Case study on the influence of synoptic-scale processes on the paired H_2 O–O_3 distribution in the UTLS across a North Atlantic jet stream, Atmospheric Chemistry and Physics, 23, 999–1018, https://doi.org/10.5194/acp-23-999-2023, 2023.

Seifert, A.: A Revised Cloud Microphysical Parameterization for COSMO-LME, COSMO Newsletter Proceedings from the 8th COSMO General Meeting in Bucharest, 2006, Consortium for Small-Scale Modelling,, pp. 25–28, http://www.cosmo-model.org, 2008.

Sharman, R. D., Trier, S. B., Lane, T. P., and Doyle, J. D.: Sources and dynamics of turbulence in the upper troposphere and lower stratosphere: A review, Geophysical Research Letters, 39, 2012GL051 996, https://doi.org/10.1029/2012GL051996, 2012.

Singh, S., Schmidli, J., Bašták Ďurán, I., and Westerhuis, S.: Impact of the Turbulence Parameterization on Simulations of Fog Over Complex Terrain, Journal of Geophysical Research: Atmospheres, 130, e2024JD042 610, https://doi.org/10.1029/2024JD042610, 2025.

Ďurán, I. B., Geleyn, J.-F., Váňa, F., Schmidli, J., and Brožková, R.: A Turbulence Scheme with Two Prognostic Turbulence Energies, Journal of the Atmospheric Sciences, 75, 3381–3402, https://doi.org/10.1175/JAS-D-18-0026.1, 2018.

Ďurán, I. B., Sakradzija, M., and Schmidli, J.: The Two-Energies Turbulence Scheme Coupled to the Assumed PDF Method, Journal of Advances in Modeling Earth Systems, 14, e2021MS002 922, https://doi.org/10.1029/2021MS002922, 2022.

Voelker, G. S.: MS-GWaM: A Three-Dimensional Transient Gravity Wave Parametrization for Atmospheric Models, JOURNAL OF THE ATMOSPHERIC SCIENCES, 81, 2024.

Wratt, D. S., Ridley, R. N., Sinclair, M. R., Larsen, H., Thompson, S. M., Henderson, R., Austin, G. L., Bradley, S. G., Auer, A., Sturman, A. P., Owens, I., Fitzharris, B., Ryan, B. F., and Gayet, J.-F.: The New Zealand Southern Alps Experiment, Bulletin of the American Meteorological Society, 77, 683–692, https://doi.org/10.1175/1520-0477(1996)077<0683:TNZSAE>2.0.CO;2, 1996.

Zängl, G., Reinert, D., Rípodas, P., and Baldauf, M.: The ICON (ICOsahedral Non-hydrostatic) modelling framework of DWD and MPI-M: Description of the non-hydrostatic dynamical core, Quarterly Journal of the Royal Meteorological Society, 141, 563–579, https://doi.org/10.1002/qj.2378, _eprint: https://onlinelibrary.wiley.com/doi/pdf/10.1002/qj.2378, 2015.